JACS
JOURNAL OF THE AMERICAN CHEMICAL SOCIETY
Communication
pubs.acs.org/JACS

Effect of Nature and Location of Defects on Bandgap Narrowing in Black TiO_2 Nanoparticles

Alberto Naldoni,*[,†] Mattia Allieta,[§] Saveria Santangelo,[‡] Marcello Marelli,[†] Filippo Fabbri,[#] Serena Cappelli,[§] Claudia L. Bianchi,[§] Rinaldo Psaro,[†] and Vladimiro Dal Santo*[,†]

[†]CNR−Istituto di Scienze e Tecnologie Molecolari, Via C. Golgi 19, Milano 20133, Italy
[§]Dipartimento di Chimica Fisica ed Elettrochimica, Università degli Studi di Milano, Via Golgi 19, Milano 20133, Italy
[‡]Dipartimento di Meccanica e Materiali, Università "Mediterranea" di Reggio Calabria, Loc. Feo di Vito, 89122 Reggio Calabria, Italy
[#]IMEM-CNR Institute, Parco Area delle Scienze 37/A, 43100 Parma, Italy

Supporting Information

ABSTRACT: The increasing need for new materials capable of solar fuel generation is central in the development of a green energy economy. In this contribution, we demonstrate that black TiO_2 nanoparticles obtained through a one-step reduction/crystallization process exhibit a bandgap of only 1.85 eV, which matches well with visible light absorption. The electronic structure of black TiO_2 nanoparticles is determined by the unique crystalline and defective core/disordered shell morphology. We introduce new insights that will be useful for the design of nanostructured photocatalysts for energy applications.

Understanding the electronic properties of reduced titanium dioxides (TiO_2) is the focus of intense current interest. Compared to bare TiO_2, defective TiO_2 is more attractive for photovoltaics,[1] photocatalysis,[2] and fuel cells owing to its narrower bandgap (less than typical 3 eV value), enabling absorption of visible light, and relatively high electrical conductivity.[3] Indeed, bandgap engineering is a crucial requirement for optimizing TiO_2 solar light harvesting capability. Several attempts involved adding metal[4,5] or nonmetal[6−8] impurities. However, the introduction of dopants, acting as charge carrier recombination centers, is a major issue affecting the photocatalytic efficiency.[9] Recently, appealing approaches based on dopant-free, pure TiO_2 phase were proposed in order to overcome this limitation.[2,10−12] Tao et al. synthesized a new phase, with bandgap of only 2.1 eV, forming at the surface of rutile TiO_2 (011) by oxidation of bulk Ti interstitials.[11] Chen et al. obtained black TiO_2 nanoparticles (NPs) with ∼1.0 eV bandgap through high-pressure hydrogenation of crystalline TiO_2.[2] Self-doping with Ti^{3+} bulk species was also demonstrated.[12] Cited examples show the decisive role of surface disorder[2] and point defects, such as oxygen vacancies (V_O's)[12] and Ti interstitial,[13] in dictating the bandgap narrowing in TiO_2.

Herein, we present the structural and electronic analysis of novel core−shell black TiO_2 NPs with a reduced bandgap obtained via a one-step crystallization/reduction process. The experimental evidence clearly identifies the nature and location of the defects introduced in the lattice of black TiO_2 NPs and their role in bandgap narrowing.

A high surface area (BET surface area ≥ 500 m^2/g) amorphous TiO_2 was chosen as a precursor for facilitating gas diffusion into TiO_2 and interaction with its structure.[14]

White TiO_2 was obtained by heating of the precursor under O_2 flow (Figure S1) at 500 °C for 1 h. Under the same conditions, black TiO_2 powder (Figure 1a), stable in air over 10 months, was obtained by precursor heating under H_2 stream, followed by fast cooling in inert environment until room temperature (RT). The use of very slow cooling rate or instantaneous exposure to air resulted in a gray coloration, hinting at a (heat- or oxygen-induced) rearrangement of the TiO_2 lattice into a more stoichiometric form. Therefore, it is argued that freezing of a metastable defective phase is the mechanism leading to the formation of black TiO_2 NPs. In fact, reducing crystalline samples (white TiO_2 and P25 Degussa) generated only pale blue colored powders with unmodified absorption spectra (Figure S2).

Diffusive reflectance UV−vis spectroscopy (Figure S2) revealed that the optical bandgap of white TiO_2 was 3.15 eV, whereas the UV onset of black TiO_2 absorption occurred at ∼2.75 eV (Table S1). In the latter, a broad absorption, starting at ∼400 nm and extending in the near-infrared (NIR) region of the spectrum, was also noted, which gave it the black coloration.

Aiming to clarify the physical origin of the visible−NIR light absorption of black TiO_2, its structural, luminescence, and electronic properties were investigated by using a combination of advanced characterization tools.

Figures S1 and 1a show synchrotron X-ray powder diffraction (SXRPD) patterns of white and black TiO_2 samples, respectively. TiO_2 produced in O-rich conditions was 100% anatase (A), whereas black TiO_2 NPs presented 81% A and 19% rutile (R) phases (Tables S2 and S3). Both samples were highly crystalline, with average particle size of 15 nm (white TiO_2) and 23 nm (black TiO_2) for the A phase.

Interestingly, reduction of TiO_2 at 400 and 450 °C generated samples that were 100% A, with unaltered absorption features (Figures S2 and S3, Table S1).

Received: February 8, 2012
Published: April 21, 2012

   dx.doi.org/10.1021/ja3012676 | J. Am. Chem. Soc. 2012, 134, 7600−7603

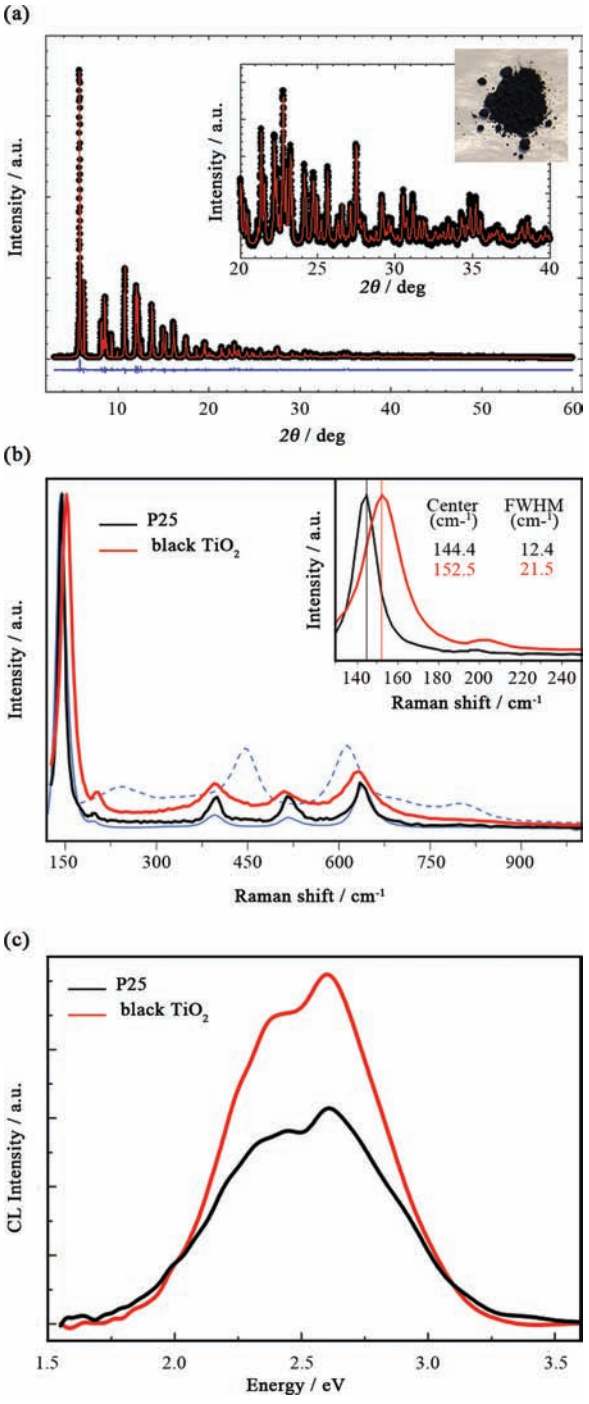

Figure 1. (a) SXRPD pattern and picture of black TiO_2 samples. (b) Micro-Raman spectra of P25 Degussa and black TiO_2. Reference spectra of pure anatase and rutile phases (continuous and dashed blue lines, respectively) are also shown. Inset: the most intense E_g peak of anatase TiO_2 for both, along with corresponding peak center positions and widths. (c) CL spectra of P25 and black TiO_2.

In the O-rich regime, the temperature of the A-to-R phase transition exceeds 700 °C, while upon our reduction conditions it drops to 500 °C. It is known that annealing in a reducing environment creates point defects in the TiO_2 crystal structure: the interaction between TiO_2 host matrix and hot H_2 molecule gives rise to V_O's that overcome the activation energy of TiO_2 lattice rearrangement and accelerate it.[15]

From the Rietveld refinement of the black sample SXRPD data, the factional occupancy of Ti and O sites in the A phase was obtained (Table S3). The absence of structural anomaly in R phase suggested a weak contribution of this phase to the overall sample properties. For the A phase, the occupation factor of O was ∼0.95, which corresponds to a V_O concentration of 5% in black sample.

Structural properties of black TiO_2 were further examined by measuring Raman scattering. Analysis was carried out also on P25 Degussa that has the same phase composition. The six ($3E_g$ + $2B_{1g}$ + A_{1g}) Raman-active modes of A phase were detected in both investigated samples (Figure 1b).[16] Since black TiO_2 spectral features were superimposed to a V_O-related photoluminescence band (Figure S5),[17] the light emission properties were studied by cathodoluminescence (CL) spectroscopy. CL spectra of both P25 and black TiO_2 (Figure 1c) show a broad structured band arising from three different radiative transitions (Figure S6), two (at 2.63 and 2.36 eV) related to V_O intragap states,[17] and one (at 2.77 eV) attributed to the self-trap exciton emission.[17] The higher intensity of V_O-related emissions in the black TiO_2 spectrum is evidence of the higher concentration of V_O's in this sample.

Finite size of the grains (<10 nm) or shortening of the correlation length because of the presence of defects results in phonon confinement effects.[18,19] Theoretical calculations show that phonon confinement leads to the blue-shift and broadening of the most intense E_g peak with respect to bulk A.[19] The smallest between correlation length of the phonons and particle size ultimately determines the Raman spectral change.[18] Here, the size of crystallites resulting from SXRPD data (23 nm) ruled out the occurrence of finite-size effects, indicating that structural disorder[2,19] (localized defects associated with V_O's) was rather responsible for the large blue-shift and broadening of the peak observed in black TiO_2 (see position and fwhm in inset of Figure 1b).

HRTEM images and related fast Fourier transform (FFT) provided detailed information on the structure of TiO_2 samples. FFTs reported in Figure 2b,c provided evidence that in some region of the sample, A and R phases have grown separately in different NPs of black TiO_2. From the FFT (inset c2) related to a well-formed A nanocrystal reported in Figure 2c, a set of

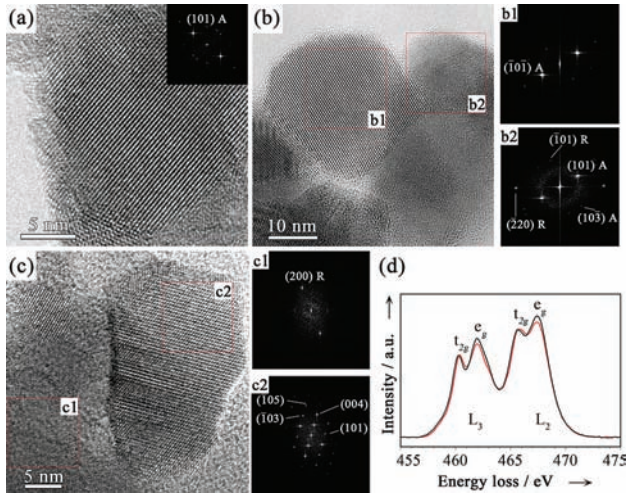

Figure 2. HRTEM micrographs of white (a) and black (b,c) TiO_2 along with their FFT shown in the insets. (c) EELS spectra of the Ti–$L_{2,3}$ edge for white (black line) and black (red line) TiO_2.

dx.doi.org/10.1021/ja3012676 | J. Am. Chem. Soc. 2012, 134, 7600–7603

interplanar distances were calculated. These distances obtained at the local scale were compared with the average ones (from SXRPD), and a contraction of about 1−4% was found. This result is consistent with a lattice contraction induced by the presence of V_O's in the A black TiO_2 structure. Remarkably, only black TiO_2 NPs presented a unique core−shell morphology characterized by a ∼1.5 nm thick disordered surface layer (Figure 2b and SI).[2]

The reduction of TiO_2 results in samples with V_O's (TiO_{2-x}) or Ti interstitials ($Ti_{1+x}O_2$). In both cases, (i) Ti is in excess with respect to O, and (ii) reduction is accompanied by the appearance of Ti^{3+} species.[20,21]

Electron energy loss near-edge structure (ELNES) appears above the absorption edge in the electron energy loss spectrum (EELS) and allows a qualitative interpretation of electronic states. O K-edges (Figure S11) and Ti L-edges are the main features present in the TiO_2 spectrum. The Ti $L_{2,3}$-edge shown in Figure 2d mainly reflects Ti 3d unoccupied states split into the t_{2g} and e_g sub-bands because of the octahedral coordination of Ti atoms with O.[22] Comparing white and black TiO_2, the $t_{2g}-e_g$ splitting is 1.69 eV vs 1.61 eV in L_3 and 1.78 eV vs 1.45 eV in L_2. The noteworthy 20% decrease observed for the L_2 peak splitting in black TiO_2 can be related to the presence of Ti^{3+} in its lattice. In fact, $t_{2g}-e_g$ states are extremely sensitive to the presence of point defects.[23] With the increase of d electrons, which corresponds to the decrease of the formal charge of the Ti ion (i.e., formation of Ti^{3+}), the occupation number of the antibonding orbital increases. As a matter of fact, the $t_{2g}-e_g$ splitting becomes smaller. Other titanium oxides, such as Ti_2O_3 or TiO, with their rather featureless ELNES,[22] are representative examples for this situation.

The presence of Ti^{3+} centers in the black TiO_2 structure was confirmed by electron paramagnetic resonance spectroscopy (Figure S12).[24−27] Interestingly, the absence of the superoxide (O_2^-) radical signal would indicate that no Ti^{3+} is present at the surface. Thus, Ti^{3+} is present exclusively in the bulk, which is a key factor for the observed stability of black TiO_2 NPs.

X-ray photoelectron spectroscopy (XPS) analysis of Ti 2p and O 1s regions evidenced no significant differences in the NP surface of P25 and black TiO_2 (Figure S13, Table S4). The Ti region was regular, and the binding energy ($Ti\_2p_{3/2}$ = 458.3 ± 0.2 eV) compared well with data for Ti^{IV} in TiO_2.[28] The O 1s peaks of P25 and black TiO_2 showed, as often reported in the case of oxides, the presence of two components, attributed to lattice oxygen (O_L) in TiO_2 (529.5 ± 0.2 eV) and to surface OH (O_{OH}) species (531.0 ± 0.2 eV).[28] The shell of black TiO_2 might originate during the fast cooling step, which freezes, as highly reactive and disordered phase, the outer surface layers (∼1.5 nm). Upon exposure to air at RT, the metastable shell can subsequently become nearly stoichiometric and preserves the nanocrystal core from further oxidation.

In our case, SXRPD and CL analyses revealed that Ti^{3+} species in black TiO_2 NPs obtained by mild thermal treatment are due to the presence of V_O's. The presence of interstitial Ti ions, most probably formed under more severe conditions (i.e., high-temperature vacuum annealing),[11,13,20,21] was ruled out since in the O-poor regime the formation of V_O's should be energetically favored compared to that of interstitial Ti ions.[29,30]

Figure 3 reports valence band (VB) XPS of reference (P25) and defective (black) TiO_2. P25 Degussa displayed the characteristic VB density of states (DOS) of TiO_2, with the band edge at ∼1.2 eV below the Fermi energy. Since the optical

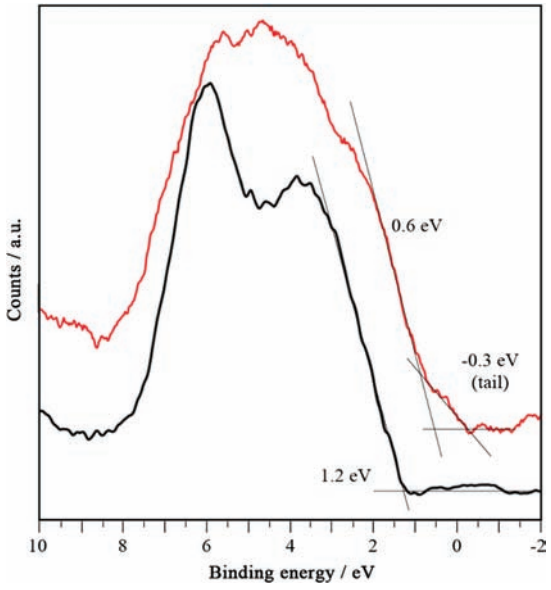

Figure 3. Valence band XPS spectra of P25 Degussa (black line) and black TiO_2 (red line). Thin black lines show the linear extrapolation of the curves used for deriving the band edge position of TiO_2 samples.

bandgap of P25 is 3.25 eV (Table S1), the conduction band (CB) minimum would occur at −2.05 eV.[2] On the other hand, VB XPS of black TiO_2 showed notable differences: the main absorption onset was located at 0.6 eV, whereas the maximum energy associated with the band tail blue-shifted further toward the vacuum level at about −0.3 eV.

Chen et al. reported that surface disorder induces a substantial shift (2.18 eV) of the VB position for hydrogenated black TiO_2 NPs,[2] while Wang et al. recently showed very similar VB spectra for both TiO_2 and TiO_2 hydrogenated nanowires.[1] Hydrogenation conditions and crystallinity of TiO_2 are key parameters in the reduction process. In our case, starting from an amorphous precursor addresses the formation of TiO_2 NPs having crystalline and defective core and disordered shell, with a peculiar DOS structure (Figure 4). If for black TiO_2 the same CB energy shape is assumed as for P25, the surface disorder induces a remarkable bandgap narrowing (1.85 eV). This value further reduces considering an already predicted slight CB tailing.[2] Furthermore, V_O's introduce localized states at 0.7−1.0 eV below the CB minimum of black TiO_2.[12,21] Therefore, electronic transitions from both tailed VB and V_O localized states to CB, and from tailed VB to V_O localized states, are responsible for the black TiO_2 vis−NIR absorption.

In summary, we have shown that our black TiO_2 NPs exhibit unique crystalline core/disordered shell morphology. V_O's are present in the bulk anatase crystalline phase, while the disordered NP surface appears to be nearly stoichiometric. The bandgap narrowing is dictated by the synergistic presence of V_O's and surface disorder. The findings of this work provide new insights for developing nanostructures tailored for solar fuel generation devices and other applications via controlled bandgap engineering.

dx.doi.org/10.1021/ja3012676 | J. Am. Chem. Soc. 2012, 134, 7600−7603

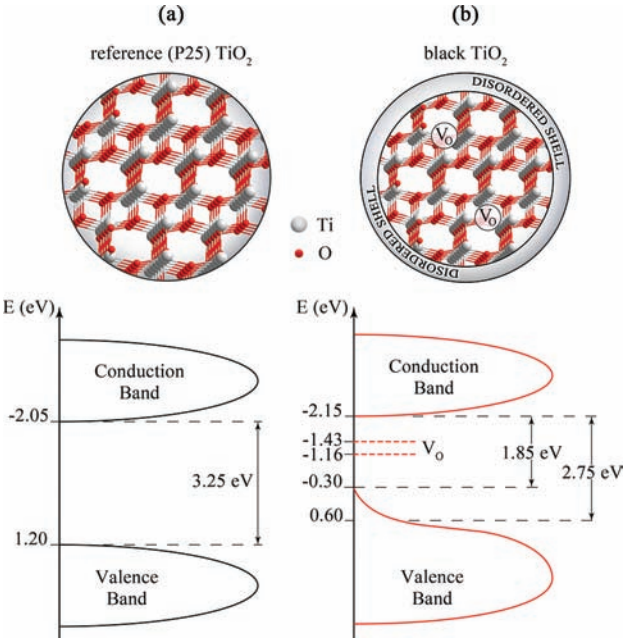

Figure 4. Schematic of nanoparticle's structure and DOS for (a) TiO_2 P25 Degussa and (b) black TiO_2. Both representations were built using experimental data from SXRPD, CL, UV–vis spectroscopy, and XPS analysis. The energy positions of V_O localized states were calculated by subtracting components at 2.36 and 2.63 eV of black TiO_2 CL band from the valence band maximum in reference TiO_2.

■ ASSOCIATED CONTENT

Ⓢ Supporting Information

Detailed synthesis, experimental methods, and additional materials characterization. This material is available free of charge via the Internet at http://pubs.acs.org.

■ AUTHOR INFORMATION

Corresponding Author

a.naldoni@istm.cnr.it; v.dalsanto@istm.cnr.it

Notes

The authors declare no competing financial interest.

■ ACKNOWLEDGMENTS

Financial support from Regione Lombardia through the project "ACCORDO QUADRO Regione Lombardia e CNR per l'attuazione di programmi di ricerca e sviluppo" and from the Italian Ministry of Education, University and Research through the FIRB Projects "ItalNanoNet" (RBPR05JH2P) and "Oxides at the nanoscale: multifunctionality and applications" (RBAP115AYN) is gratefully acknowledged. We acknoledge Dr. Adrian Hill for assistance at ID31 beamline.

■ REFERENCES

(1) Wang, G.; Wang, H.; Ling, Y.; Tang, Y.; Yang, X.; Fitzmorris, R. C.; Wang, C.; Zhang, J. Z.; Li, Y. *Nano Lett.* **2011**, *11*, 3026.

(2) Chen, X.; Liu, L.; Yu, P. Y.; Mao, S. S. *Science* **2011**, *331*, 746.

(3) Han, W. Q.; Zhang, Y. *Appl. Phys. Lett.* **2008**, *92*, 203117.

(4) Hoffmann, M. R.; Martin, S. T.; Choi, W.; Bahnemann, D. W. *Chem. Rev.* **1995**, *95*, 69.

(5) Choi, W.; Termin, A.; Hoffmann, M. R. *Angew. Chem.* **1994**, *106*, 1148.

(6) Chen, X.; Burda, C. *J. Am. Chem. Soc.* **2008**, *130*, 5018.

(7) Asahi, R.; Morikawa, T.; Ohwaki, T.; Aoki, K.; Taga, Y. *Science* **2001**, *293*, 269.

(8) Khan, S. U. M.; Al-Shahry, M.; Ingler, W. B., Jr. *Science* **2002**, *297*, 2243.

(9) Choi, W.; Termin, A.; Hoffmann, M. R. *J. Phys. Chem.* **1994**, *98*, 13669.

(10) Ariga, H.; Taniike, T.; Morikawa, H.; Tada, M.; Min, B. K.; Watanabe, K.; Matsumoto, Y.; Ikeda, S.; Saiki, K.; Iwasawa, Y. *J. Am. Chem. Soc.* **2009**, *131*, 14670.

(11) Tao, J.; Luttrell, T.; Batzill, M. *Nat. Chem.* **2011**, *3*, 296.

(12) Zuo, F.; Wang, L.; Wu, T.; Zhang, Z.; Borchardt, D.; Feng, P. *J. Am. Chem. Soc.* **2010**, *132*, 11856.

(13) Wendt, S.; Sprunger, P. T.; Lira, E.; Madsen, G. K. H.; Li, Z.; Hansen, J. Ø.; Matthiesen, J.; Blekinge-Rasmussen, A.; Lægsgaard, E.; Hammer, B.; Besenbacher, F. *Science* **2008**, *320*, 1755.

(14) Gallo, A.; Marelli, M.; Psaro, R.; Gombac, V.; Montini, T.; Fornasiero, P.; Pievo, R.; Dal Santo, V. *Green Chem.* **2012**, *14*, 330.

(15) Salari, M.; Konstantinov, K.; Liu, H. K. *J. Mater. Chem.* **2011**, *21*, 5128.

(16) Santangelo, S.; Messina, G.; Faggio, G.; Donato, A.; De Luca, L.; Donato, N.; Bonavita, A.; Neri, G. *J. Solid State Chem.* **2010**, *183*, 2451.

(17) Lei, Y.; Zhang, L. D.; Meng, G. W.; Li, G. H.; Zhang, X. Y.; Liang, C. H.; Chen, W.; Wang, S. X. *Appl. Phys. Lett.* **2001**, *78*, 1125.

(18) Zhu, K. R.; Zhang, M. S.; Chen, Q.; Yin, Z. *Phys. Lett. A* **2005**, *340*, 220.

(19) Gupta, S. K.; Desai, R.; Jha, P. K.; Sahoo, S.; Kirinc, D. *J. Raman Spectrosc.* **2010**, *41*, 350.

(20) Finazzi, E.; Di Valentin, C.; Pacchioni, G. *J. Phys. Chem. C* **2009**, *113*, 3382.

(21) Finazzi, E.; Di Valentin, C.; Pacchioni, G.; Selloni, A. *J. Chem. Phys.* **2008**, *129*, 154113.

(22) Yoshiya, M.; Tanaka, I.; Kaneko, K.; Adachi, H. *J. Phys.: Condens. Matter* **1999**, *11*, 3217.

(23) Diebold, U. *Surf. Sci. Rep.* **2003**, *48*, 53.

(24) Gopal, N. O.; Lo, H. H.; Sheu, S. C.; Ke, S. C. *J. Am. Chem. Soc.* **2010**, *132*, 10982.

(25) Berger, T.; Sterrer, M.; Diwald, O.; Knozinger, E.; Panayotov, D.; Thompson, T. L.; Yates, J. T., Jr. *J. Phys. Chem. B* **2005**, *109*, 6061.

(26) D'Arienzo, M.; Carbajo, J.; Bahamonde, A.; Crippa, M.; Polizzi, S.; Scotti, R.; Wahba, L.; Morazzoni, F. *J. Am. Chem. Soc.* **2011**, *133*, 17652.

(27) Livraghi, S.; Maurelli, S.; Paganini, M. C.; Chiesa, M.; Giamello, E. *Angew. Chem., Int. Ed.* **2011**, *4*, 1.

(28) Cappelletti, G.; Ardizzone, S.; Bianchi, C. L.; Gialanella, S.; Naldoni, A.; Pirola, C.; Ragaini, V. *Nanoscale Res. Lett.* **2009**, *4*, 97.

(29) Janotti, A.; Varley, J. B.; Rinke, P.; Umezawa, N.; Kresse, G.; Van de Walle, C. G. *Phys. Rev. B* **2010**, *81*, 085212.

(30) Morgan, B. J.; Watson, G. W. *J. Phys. Chem. C* **2010**, *114*, 2321.